IEEE Access
Multidisciplinary | Rapid Review | Open Access Journal

Received April 30, 2019, accepted May 24, 2019, date of publication May 29, 2019, date of current version June 12, 2019.

Digital Object Identifier 10.1109/ACCESS.2019.2919684

Model Predictive Iterative Learning Control for Energy Management of Plug-In Hybrid Electric Vehicle

HONG-QIANG GUO[1], CONG-ZHI LIU[2], JIA-WANG YONG[2], XING-QUN CHENG[1], AND FAHAD MUHAMMAD[2]

[1]School of Mechanical and Automotive Engineering, Liaocheng University, Shandong 252000, China
[2]State Key Laboratory of Automotive Safety and Energy, Tsinghua University, Beijing 100084, China

Corresponding author: Jia-Wang Yong (yongjw@tsinghua.edu.cn)

This work was supported in part by the National Key Research and Development Program of China under Grant 2017YFB0103502 and in part by the National Science Fund of the People's Republic of China under Grant 51675293.

ABSTRACT A novel optimal energy management strategy (EMS) for plug-in hybrid electric vehicle (PHEV) is proposed in this paper, which takes the battery health into consideration for prolonging its service life. The integrated control framework combines batch-wise iterative learning control (ILC) and time-wise model predictive control (MPC), referred to as 2D-MPILC. The major advantages of the proposed method are shown with better performance as well as faster convergence speed by taking into account the time-wise feedback control within the current batch. Then, the MPILC method is applied for the PHEV with the ability to make continuous period-to-period improvements. Its performances will approach dynamic programming (DP)-based method after a learning process with satisfying real-time processing capacity. The results in real-world city bus routines verify the effectiveness of the proposed EMS for greatly improving the performance of the PHEV.

INDEX TERMS Plug-in hybrid electric vehicle, model predictive iterative learning control, battery aging, nonlinear optimization, 2-D Lyapunov stability theory.

I. INTRODUCTION

Recently, electric vehicles (EVs), hybrid electric vehicles (HEVs) and plug-in hybrid electric vehicles (PHEVs) have been widely studied and used due to their potential to reduce fuel consumption (FC) and emissions [1], [2]. However, it is still a difficult issue to distribute the demand power between the fuel-based and electricity-based power sources. Moreover, the engine cannot always operate with high efficient. Accordingly, further research of energy management strategy (EMS) which enables the HEVs to operate efficiently during complex driving cycles is challenging [3], [4]. Furthermore, as the driving conditions of city running vehicles (such as bus, delivery vehicle) are repetitive, the historical traffic and driving cycles information can be utilized to enhance the energy efficiency [5]. Therefore, it is a meaningful research work to seek an effective EMS for HEVs or PHEVs.

The associate editor coordinating the review of this manuscript and approving it for publication was Md Asaduzzaman.

The methods related to EMS for HEVs and PHEVs can be generally divided into 'rule-based' and 'optimization-based' strategies. The rule-based EMS can be applied easily in real vehicles [6], [7]. The optimization-based strategies are performed for the optimal energy management problem [8]–[10]. It is well known that the model predictive control (MPC) method has been widely used due to it can achieve an optimal performance for the power split [11]–[13]. For example, an MPC-based EMS was proposed for a PHEV to improve the real-time implementation performance [14]. However, some factors are required to be fully considered to improve the performance, for instance:

Driver Behavior: To optimize the performance of overall system, the driver behavior must be considered [15], [16]. Because the PHEV usually runs in fixed route which has repetitiveness of the city route and similar terrain of a certain region, the stochastic feature of driver behavior can be obtained from the historical driving data [17]. Then, the driver models were introduced to EMS [18], [19].

Battery Aging: During driving operations, batteries undergo several cycles of charging and discharging in a relatively short time, which will contribute to accelerating the battery aging process and decreasing the battery lifetime [20]. Accordingly, battery health is an important aspect and should be paid enough attention to the EMS [21]–[23]. For example, an optimal EMS including battery aging was proposed [24]. A new cost-optimal control framework was constructed to minimize the daily operational expense of a PHEV [25].

Iterative Learning: When PHEV runs on a fixed route, the same dynamic errors will show up over and over as the same operations are repeated with the traditional MPC [26]. Learning from experience is important to improve performance, so, monitoring the running states of PHEV in previous days is useful to improve performances for the next time [27], [28]. Inspired by this idea, the iterative learning technique can be developed as an alternative approach, where the learning is intuitively considered as a bridge between knowledge and experience: that is to say the lack of knowledge is compensated by experience.

It is well known that the iterative learning control (ILC) theory is a powerful tool for dynamical systems with repetitive operation due to its ability to adjust the control input from batch to batch [29], [30]. Also, it has been applied in many processes not strictly repetitive, such as the boiler-turbine system [31] and the non-repetitive trajectory tracking of mobile robots [32]. Additionally, the ILC technique can be combined with a predictive control technique. For example, an MPC utilizes the repetitive nature of batch operation and performs batch-wise feedback together with real-time predictive control [33]. A combination of MPC and ILC was proposed to not only speed up the response time but also effectively reduce the speed ripples [34]. To reduce FC and alleviate battery degradation simultaneously, an effective EMS should be designed for PHEV by using more of the past control information. It motivates us to make some attempts.

A novel model predictive iterative learning control (MPILC) is proposed to achieve an optimal performance in the repetitive process with the key idea of 'practice makes perfect' that is an extension of ILC and optimum control. When the PHEV is operated repeatedly in the finite time interval, the opportunity exists in the MPILC to improve the control performance in the next iteration based on the observation of the previous attempts. Therefore, the main objective of this paper is to design an MPILC-based EMS that takes the battery aging into consideration. Compared to the existing literatures, the main contributions lie in the followings:

Contribution 1: For the PHEV usually running on a fixed route, the driver behavior is predictable based on a high-order internal model (HOIM). Then, the optimal torque split problem is transformed into an MPILC design problem of a 2-D Roesser model with non-zero boundary condition.

Contribution 2: The MPILC design criteria based on 2-D Lyapunov stability theory is established to achieve perfect tracking and guaranteed cost performances.

Contribution 3: A semi-empirical battery aging model is established and introduced into the EMS. Then, the power split strategy for the motor and engine of PHEV is abstracted as a nonlinear dynamic optimization problem with constraints to balance the FC and battery aging.

The outline of this paper is as follows. Section II develops the system models incorporating the PHEV model and battery aging model. Section III formulates the MPILC-based EMS with considering battery aging. The main results of the proposed EMS are discussed in section IV. Finally, the main contributions and conclusions are summarized in section V.

Notations. Denote $\mathbb{R}^n$ the n-dimensional Euclidean space, $\mathbb{R}^{n\times m}$ the set of all $n \times m$ real matrices, $\|\cdot\|$ the usual Euclidean norm, and $\|\cdot\|_2$ the ℓ_2 norm along iterative axis, i.e., $\|\boldsymbol{w}_k(t)\|_2 = \sqrt{\sum_{k=0}^{\infty}\|\boldsymbol{w}_k(t)\|^2}$, and I_n the $n \times n$ identity matrix. For any symmetric matrix A, the inequalities $A > 0$ or $A < 0$ denote that the matrix A is positive definite or negative definite, respectively. In addition, the notation $*$ represents the elements below the main diagonal of a symmetric matrix.

II. PHEV SYSTEM ARCHITECTURE AND MODELS

Single-shaft parallel hybrid powertrain with automated mechanical transmission (AMT) is widely used in PHEV due to its compact structure and high transmission efficiency [35], [36]. The hybrid powertrain in this paper incorporates an internal combustion engine (ICE), a lithium iron phosphate battery pack with battery management system (BMS), an electric machine that can be used as both motor and generator, and an AMT, which is shown as Figure 1. The powertrain system is controlled by controller area network (CAN). The engine and motor can either drive the vehicle independently or together. Thus the PHEV can be operated in five operating modes which are EV mode, engine driving mode, hybrid driving mode, regenerative braking mode and engine active charging mode. The operating modes can be switched by the engagement and disengagement of the automatic clutch between the engine and motor, but the multi-power sources are highly coupled in power-split process [37]. The efficiency of the hybrid powertrain system can be improved by the automatic gear shifting of the AMT. The main parameters are listed in Table 1.

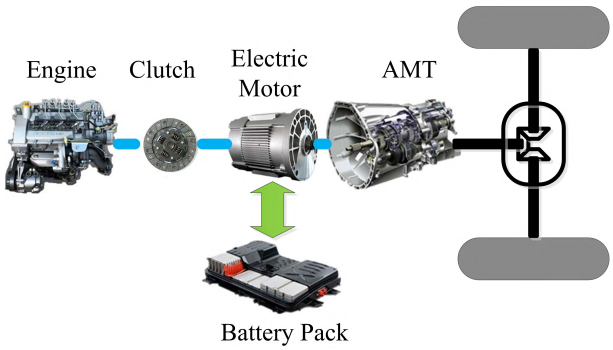

FIGURE 1. The structure of the PHEV powertrain system.

TABLE 1. Main parameters of the bus.

Component	Descriptions
ICE	Product model:YC6J200-42, displacement:6.494L, nominal power:147kw
Motor	Max torque:750Nm, nominal power:55kw, peak power:95kw
Battery	Lithium iron phosphate,capacity:40Ah,voltage:359V
AMT	6-speed, gear ratio: 6.39/3.97/2.4/1.48/1/0.73
Vehicle	Length: 10.5(m),empty mass: 11980 (kg)

A. BASIC DYNAMIC MODEL OF THE PHEV

The longitudinal vehicle dynamic characteristic can be described as followings:

$$\delta m\frac{dV}{dt} = \frac{T_d}{r_w} - \frac{1}{2}c_d\rho_a AV^2 - mg(\mu_r\cos\beta + \sin\beta) \quad (1)$$

$$T_d = \eta_T \cdot i_g \cdot i_{fd}\,(T_e + T_m) + T_b, \quad (2)$$

where m, δ, g, r_w, μ_r, β, c_d, A, ρ_a, V and T_d denote the vehicle mass, conversion factor of the vehicle mass ($\delta > 1$), gravity acceleration, wheel radius, rolling resistance, road grade, air drag coefficient, front area, air density, vehicle speed and wheel torque, respectively. η_T, i_g, i_{fd}, T_e, T_m and T_b denote the transmission efficiency, gear ratio of the AMT, final drive ratio, engine torque, motor torque and mechanic braking torque on wheels, respectively. Note that mechanic braking torque T_b is the torque from conventional friction brakes, in case that regenerative braking is not sufficient to provide the desired braking torque. If the engine and motor operate in hybrid driving mode, the relationship between the rotational angular velocity of the driving wheels and that of the two power sources is:

$$\omega_{wheel} = \frac{\omega_e}{i_g i_{fd}} = \frac{\omega_m}{i_g i_{fd}} \quad (3)$$

where ω_{wheel}, ω_e and ω_m are rotational speed of driving wheels, engine and electric motor, respectively.

B. INTERNAL COMBUSTION ENGINE MODEL

Since only FC of the engine is taken into consideration, the complex dynamic characteristics are neglected. The engine's FC rate is written as:

$$\dot{m}_f = \frac{T_e\omega_e \cdot b_e(\omega_e, T_e)}{3600\rho_f} \quad (4)$$

where $\dot{m}_f$ and ρ_f are the FC rate and diesel density, respectively. $b_e(\omega_e, T_e)$ is a MAP which denotes the brake specific FC (BSFC) of engine.

C. ELECTRIC MOTOR MODEL

When the electric machine is acting as a motor, it will draw energy from the battery and provide propulsion together with the engine. Correspondingly, when it is acting as a generator, it will charge the battery in engine active charging mode or regenerative braking mode. The demand power of electric motor can be given as:

$$P_m = \frac{T_m\omega_m}{(\eta_m)^{sgn(T_m)}} \quad (5)$$

where sgn$(*)$ denotes the sign function. The efficiency of the electric motor $\eta_m(\omega_m, T_m)$ is a MAP which could be obtained according to ω_m and T_m.

D. EQUIVALENT CIRCUIT MODEL OF THE BATTERY

Battery modeling plays an important role and many researches have been conducted, such as H_∞ switched observer for state of charge (SOC) estimation [38], state of health (SOH) evaluation [39] and comparison study of different battery models [40]. In fact, the critical state to the power management is the slowly varying SOC of the battery [41]. Therefore, a control-oriented battery model is simplified as followings [17]

$$\begin{cases} S\dot{O}C = -I_{batt}/Q_{batt}, \\ P_{batt} = U_{oc}I_{batt} - RI_{batt}^2, \end{cases} \quad (6)$$

which can be rewritten as:

$$S\dot{O}C = \frac{-U_{oc} + \sqrt{U_{oc}^2 - 4P_{batt}R}}{2Q_{batt}R}, \quad (7)$$

where Q_{batt}, U_{oc}, R and P_{batt} denote the capacity, open circuit voltage, internal resistance and output power of the battery, respectively. Note that U_{oc} and R could be obtained according to SOC and temperature.

E. BATTERY AGING MODEL

The real driving cycle could cause the battery operating in serious conditions occasionally. So, it is important to take the battery aging into consideration during the optimum control process. A semi-empirical control-oriented aging model is applied for the battery degradation [42], which is evaluated by the normalized battery capacity loss Q_{loss} as:

$$Q_{loss}(I_c, \theta, C_{Ah}) = \left[1 - \frac{\sigma_f(I_c, \theta)\cdot(C_{Ah})^z}{Q_{batt}}\right]\cdot 100\%, \quad (8)$$

$$\sigma_f(I_c, \theta) = \alpha \cdot \exp\left(\frac{-E_a + \eta I_c}{R_g(273.15 + \theta)}\right), \quad (9)$$

where θ, Q_{batt} and C_{Ah} denote the temperature, nominal capacity, accumulated charge throughput, respectively. z is power law exponent that represents Ah-throughput dependence. $\sigma_f(I_c, \theta)$ is a nonlinear severity factor function. $R_g = 8.314[Jmol^{-1}K^{-1}]$ is universal gas constant. $E_a = 31500[Jmol^{-1}]$ is activation energy. The current rate I_c is defined as $I_c = |I|/Q_{batt}$ and its unit is 1/h (per hour).

The severity factor map $\sigma_{map}(I_c, \theta)$ characterizes the relative aging of a battery under different operating conditions as [24]:

$$\sigma_{map}(I_c, \theta) = \frac{\Gamma(I_c,\theta)}{\Gamma_{c,nom}} = \frac{\int_0^{EOL}|I(t)|dt}{\int_0^{EOL}|I_{c,nom}(t)|dt} \quad (10)$$

where EOL means the end-of-life. $\Gamma(I_c, \theta)$ and $\Gamma_{c,nom}$ denote the total Ah-throughput of the battery in the given condition and nominal operating condition with $I_{c,nom} = 1[1/h]$, $\theta_{nom} = 25°$C, respectively, and it is assumed that the battery has maximum cycle life under the nominal condition.

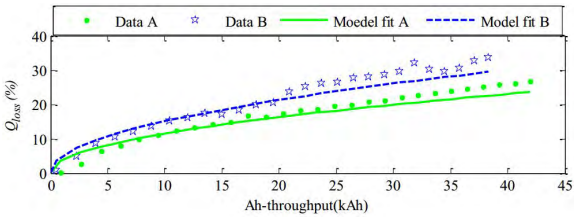

FIGURE 2. The identified battery aging model.

Battery severity map is defined as the ratio of the total accumulated Ah-throughput in nominal cycle to that of actual operating conditions until the *EOL*. With the battery aging model, the *EOL* is defined as 20% capacity loss under nominal operating condition,

$$\sigma_f(I_{c,nom}, \theta_{nom}) \cdot \Gamma^z_{c,nom} = 0.8 * Q_{batt}. \tag{11}$$

Battery cycle test is conducted on a battery test bench under the temperature $\theta = 25^oC$. Then, the parameters of battery aging model can be identified, where the current rates of data A and B are $I_{c,A} = 1[1/h]$, $I_{c,B} = 5[1/h]$, respectively. The identified parameters are $z = 0.4997$, $\eta = 32.648$, $\alpha = 77982$. The maximum battery life is $\Gamma_{c,nom} = 30.3288$kAh. As shown in Figure 2, the identified results are match closely with original test data. It is clear that the modeling error will be increased along with the Ah-throughput increased, however, the modeling accuracy is high enough for the battery application with a small Ah-throughput. According to (10)-(11), the severity factor map as shown in Figure 3 can be established, which is calculated offline with temperature and current rate as $\theta = [0, 10, 20, 30, 40]°C$, $I_c = [0, 5, 10, 15]1/h$. Then, it can play a similar role of an engine FC map when it is used in the optimization framework aimed at minimizing FC and battery degradation.

III. OPTIMAL CONTROL PROBLEM FORMULATION AND SOLUTION

Because the vehicles (including passenger cars and commercial vehicles) usually run in fixed route which has iterative repetitiveness of the route and similar terrain of a certain region, the iteration-varying feature of driver behavior can be obtained from the historical driving data. Inspired by the method [43] and according to the iterative repetitiveness of the city route, an important assumption should be given first for the MPILC-based EMS.

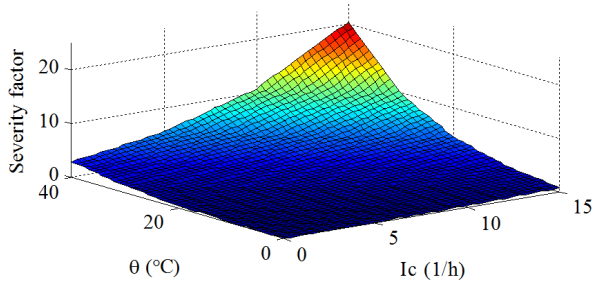

FIGURE 3. Severity factor map.

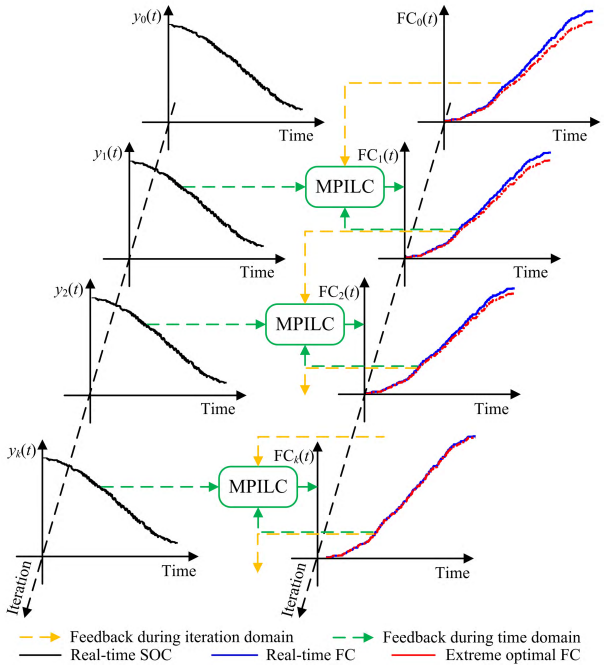

FIGURE 4. Principle of the MPILC.

Assumption 1: There exists an intrinsical characteristics of the iteration-varying features which can be defined by HOIM and are not limited to the cases on the same city route including: different vehicle, different driver, new vehicle or new driver operated on the route first.

For the classic MPC, the control law is only updated during time domain. On the contrary, for the proposed MPILC as shown in Figure 4, it is an extension of classic MPC in iteration domain, and it will be updated during time and iteration domains. It is important to point out that the system input is not only determined by batch-to-batch control but also the adjustment based on MPC. Therefore, the FC is reduced gradually along with iteration axis by iterative learning technique, and it will approach to the extreme optimal FC.

During the different operational cycles, the control target is accordant, that is to seek an optimal control law for minimizing the FC and battery fading, simultaneously. Different from conventional HEVs, the PHEV has equipped larger battery pack which can be charged from the power grid, therefore, the electric power of battery can provide a larger part of the demand energy to reduce the FC. In order to make full use of the energy from charging stations, finding a reasonable reference SOC curve is important. Clearly, one of the optimal situations is that the battery energy is just used up at the end of the driving cycle, then, the reference SOC values can be obtained from the beginning to end [17].

A. HOIM-BASED DRIVER MODEL

The driver behavior can be described as the demand torque T_d. According to assumption 1, the iteration-varying feature of driver behavior can be defined by the following definition to use more information of the historical driving data [44].

Definition 1: The driver behavior is modeled by the demand torque as

$$T_{d,k}(t) = T^r_{d,k}(t) + T^s_{d,k}(t), \tag{12}$$

and

$$\begin{cases} T^r_{d,k+1}(t) = G_\varrho(q^{-1})T_{d,k}(t), k \geq 0, \\ T_{d,k}(t) = T^0_{d,k}(t), k \leq 0, \\ \sum_{t=0}^{T} \|T^s_{d,k}(t)\|_2 < \infty, \end{cases} \tag{13}$$

where $t \in [0, T_f]$ and $k \geq 0$ represent discrete time and iterative time along with time and iteration axes, respectively. It means that $T_{d,k}(t)$ and $T^0_{d,k}(t)$ are the real-time and initial demand torques at the discrete time point t of k^{th} repetitively driving in the fixed route, respectively. $T^r_{d,k}(t)$ and $T^s_{d,k}(t)$ are iterative repetitive and stochastic parts of driver behavior, respectively. Moreover, $T^r_{d,k}(t)$ represents the iterative learning process according to the historical driving condition, and $T^s_{d,k}(t)$ represents the driver's stochastic and uncertain decision during the varying driving scene. q is a shift operator in iteration domain with the property $q^{-1}T_{d,k}(t) = T_{d,k-1}(t)$. And $G_\varrho(q^{-1})$ is a stable HOIM with the order ϱ as

$$G_\varrho(q^{-1}) = \beta_1 + \beta_2 q^{-1} + \cdots + \beta_\varrho q^{-\varrho+1}. \tag{14}$$

Then, the iterative repetitive part $T^r_{d,k}(t)$ of driver behavior can be rewritten as a linear regression form

$$\begin{aligned} T^r_{d,k+1}(t) = {} & \beta_1 T_{d,k}(t) + \beta_2 T_{d,k-1}(t) \\ & + \beta_3 T_{d,k-2}(t) + \cdots + \beta_\varrho T_{d,k-\varrho+1}(t), \end{aligned}$$

which implies that it is a linear combination of the past ϱ iterations. Hence, the driver behavior can be described by the historical driving cycles and a current stochastic varying part and it is the key to make the learning law to adapt to the varying driving cycles. According to the iterative repetitiveness and periodicity of city route within one week, i.e., 7 days, the order of HOIM $G_\varrho(q^{-1})$ can be selected as $\varrho = 7$, and to maintain the iterative consistency and predictability, $G_\varrho(q^{-1})$ satisfies

$$\sum_{i=1}^{\varrho} \beta_i = 1. \tag{15}$$

Remark 1: The definition 1 gives a description of the driver behavior, which is modeled as a summation of the working condition information in the past week and with some norm-bounded disturbances. The incorporated construction (12) is aimed to improve the varying dynamic behaviors of drivers. Due to the consideration of the stochastic driver behavior $T^s_{d,k}(t)$, it is practical for the varying traffic scenes.

As vehicles often run in a fixed-route, the HOIM that reflects the driving behavior can be extracted from large amount of historical driving data by minimizing the modeling error as following

$$\underset{\beta_i}{arg\,min}\ J = \sum_{k=0}^{30} \sum_{t=0}^{T} \|T_{d,k}(t) - T^r_{d,k}(t)\|^2, \tag{16}$$

which means that the parameters β_i can be obtained by the driving data of the past 30 iterations. In addition, via updating historical driving cycle database with vehicle running, the HOIM of driver behavior would be identified more route-specific and practical. It can not only be utilized in predictive control of PHEV but also help to mitigate traffic congestion and improve traffic flow efficiency.

Therefore, the HOIM of driver behavior plays a critical role to achieve satisfactory control performance by using the prosperities of PHEV according to the internal model principle (IMP).

B. 2-D ROESSER MODEL FOR PHEV

It is assumed that the PHEV is operated repetitively over a finite time duration $[0, T_f]$. Select the state, control input and output as:

$$\begin{cases} \boldsymbol{x}_k(t) = [SOC_k(t), V_k(t)]^T, \\ \boldsymbol{u}_k(t) = \left[T_{e,k}(t), T_{m,k}(t)\right]^T, \\ y_k(t) = SOC_k(t). \end{cases} \tag{17}$$

The discretization is applied based on first-order Taylor approximation. According to the PHEV system architecture, a nonlinear model is expressed as:

$$\begin{cases} \boldsymbol{x}_k(t+1) = \boldsymbol{x}_k(t) + \bar{B}_1 \boldsymbol{u}_k(t) + \boldsymbol{f}(\boldsymbol{x}_k(t), \boldsymbol{u}_k(t)), \\ y_k(t) = C_0 \boldsymbol{x}_k(t), \end{cases} \tag{18}$$

where the matrices and nonlinear function are

$$\bar{B}_1 = \frac{\eta_T i_g i_{fd}}{m r_w} \begin{bmatrix} 0 & 0 \\ 1 & 1 \end{bmatrix}, C_0 = \begin{bmatrix} 1 & 0 \end{bmatrix},$$

$$\boldsymbol{f}(\boldsymbol{x}_k(t), \boldsymbol{u}_k(t)) = T_s \begin{bmatrix} \frac{\sqrt{U^2_{oc,k}(t) - 4R_k(t)P_{m,k}(t)} - U_{oc,k}(t)}{2Q_{batt}R_k(t)} \\ \frac{T_b(t)}{m r_w} - \frac{1}{2m} c_d \rho_a A V^2_k(t) - g(\mu_r \cos\beta + \sin\beta) \end{bmatrix},$$

where $T_s = 0.1$s is sample time. The nonlinear function $\boldsymbol{f}(\boldsymbol{x}_k(t), \boldsymbol{u}_k(t))$ satisfies Lipschitz continuity condition. The control task is to find an appropriate input $\boldsymbol{u}_k(t)$ based on available information with the constraints:

$$\begin{cases} SOC_{\min} \leq SOC_k(t) \leq SOC_{\max}, \\ T_{e,\min}(\omega_e) \leq T_{e,k}(t) \leq T_{e\_\max}(\omega_e), \\ T_{m,\min}(\omega_m) \leq T_{m,k}(t) \leq T_{m\_\max}(\omega_m), \\ \omega_{e,\min} \leq \omega_e \leq \omega_{e,\max}, \\ \omega_{m,\min} \leq \omega_m \leq \omega_{m,\max}. \end{cases} \tag{19}$$

Assume that $SOC_r(t)$ is the iteration-invariant reference SOC and define the tracking error of $SOC_k(t)$ as

$$\begin{cases} e_k(t) = SOC_k(t) - SOC_r(t), k \geq 0, \\ e_k(t) = e_0(t), \ k \leq 0. \end{cases} \tag{20}$$

According to the iteration-varying feature of driver behavior, an HOIM-based ILC is proposed:

$$\begin{cases} \boldsymbol{u}_{k+1}(t) = G_\varrho(q^{-1})\boldsymbol{u}_k(t) + \delta \boldsymbol{u}_k(t+1), k \geq 0, \\ \boldsymbol{u}_k(t) = \boldsymbol{u}_0(t), \boldsymbol{x}_k(t) = \boldsymbol{x}_0(t), k \leq 0, \end{cases} \tag{21}$$

where $\boldsymbol{u}_0(t)$ denotes the initial input, $\delta\boldsymbol{u}_k(t)$ is the modification of the input that will be designed later.

In order to transform the nonlinear PHEV system (18) and the HOIM-based ILC (21) into a 2-D system, let

$$\begin{cases} \delta\boldsymbol{\chi}_k(t) = \boldsymbol{\chi}_{k+1}(t-1) - G_\varrho(q^{-1})\boldsymbol{\chi}_k(t-1), \\ \delta\boldsymbol{f}_k(t) = \boldsymbol{f}(\boldsymbol{x}_{k+1}(t-1), \boldsymbol{u}_{k+1}(t-1)) \\ -G_\varrho(q^{-1})\boldsymbol{f}(\boldsymbol{x}_k(t-1), \boldsymbol{u}_k(t-1)), \end{cases} \tag{22}$$

where $\boldsymbol{\chi} = \boldsymbol{x}, y$ or $\boldsymbol{u}$. Then, from (18) to (22), we can easily obtain a 2-D Roesser model [45] as

$$\begin{cases} \begin{bmatrix} \delta\boldsymbol{x}_k(t+1) \\ \hat{\boldsymbol{e}}_{k+1}(t) \end{bmatrix} = A \begin{bmatrix} \delta\boldsymbol{x}_k(t) \\ \hat{\boldsymbol{e}}_k(t) \end{bmatrix} + B_1\delta\boldsymbol{u}_k(t) + B_2\delta\boldsymbol{f}_k(t), \\ \boldsymbol{z}_k(t) = \hat{\boldsymbol{e}}_k(t) = C \begin{bmatrix} \delta\boldsymbol{x}_k(t) \\ \hat{\boldsymbol{e}}_k(t) \end{bmatrix}, \\ t \in [1, T_f], k \geq 0, \end{cases} \tag{23}$$

where $\boldsymbol{z}_k(t)$ is the controlled output, and

$$\begin{aligned} \hat{\boldsymbol{e}}_k(t) &= \left[e_k(t), e_{k-1}(t), \cdots, e_{k-\varrho+1}(t) \right]^T, \\ A &= \left[\begin{array}{c|ccc} I_2 & 0 & \dots & 0 \\ \hline C_0 & \beta_1 & \dots & \beta_\varrho \\ 0 & 1 & \dots & 0 \\ \vdots & \vdots & \ddots & \vdots \\ 0 & 0 & \dots & 1 \end{array}\right] \\ &\triangleq \begin{bmatrix} I_2 & 0 \\ A_{21} & A_{22} \end{bmatrix}, \\ B_1 &= \begin{bmatrix} \bar{B}_1 \\ ine0 \\ \vdots \\ 0 \end{bmatrix} \triangleq \begin{bmatrix} \bar{B}_1 \\ 0 \end{bmatrix}, B_2 = \begin{bmatrix} I_2 \\ ineC_0 \\ \vdots \\ 0 \end{bmatrix} \\ &\triangleq \begin{bmatrix} I_2 \\ A_{21} \end{bmatrix}, \\ C &= \left[0, I_\varrho\right]. \end{aligned}$$

Assumption 2: The 2-D Roesser model (23) satisfies the following boundary conditions

$$\|\delta\boldsymbol{x}_k(1)\|_2 < \infty, \|\hat{\boldsymbol{e}}_0(t)\|_2 < \infty. \tag{24}$$

Proposition 1: According to the condition (15) and (22), the following Lipschitz continuity condition holds:

$$\begin{aligned} \|\delta\boldsymbol{f}_k(t)\| &= \|\boldsymbol{f}(\boldsymbol{x}_{k+1}(t-1), \boldsymbol{u}_{k+1}(t-1)) \\ &\quad -G_\varrho(q^{-1})\boldsymbol{f}(\boldsymbol{x}_k(t-1), \boldsymbol{u}_k(t-1))\| \\ &\leq l_1\|\boldsymbol{x}_{k+1}(t-1) - G_\varrho(q^{-1})\boldsymbol{x}_k(t-1)\| \\ &\quad +l_2\|\boldsymbol{u}_{k+1}(t-1) - G_\varrho(q^{-1})\boldsymbol{u}_k(t-1)\| \\ &= l_1\|\delta\boldsymbol{x}_k(t)\| + l_2\|\delta\boldsymbol{u}_k(t)\|, \end{aligned} \tag{25}$$

where $l_1 > 0, l_2 > 0$.

Therefore, the control task has been changed to find a modification input $\delta\boldsymbol{u}_k(t)$ for the 2-D Roesser model (23) in order to guarantee that the 2-D closed-loop system is stable and the FC converges to its extreme optimal value.

C. MPILC LAW

Normally for the tracking problem given above, a satisfying MPILC rule can be obtained by:

$$\delta\boldsymbol{u}_k(t) = \delta\bar{\boldsymbol{u}}_k(t-1) + L[\,\delta\boldsymbol{x}_k^T(t)\ \hat{\boldsymbol{e}}_k^T(t)\,]^T, \tag{26}$$

where L is learning gain matrix. $\delta\bar{\boldsymbol{u}}_k(t)$ is within-batch control part which will be determined by MPC. When $\delta\bar{\boldsymbol{u}}_k(t) = 0$ which implies that the MPILC (26) is reduced to an ILC law from batch to batch, and it is reduced to an MPC law within the batch when $L = 0$.

From (23) and (26), the PHEV system based on 2-D Roesser model can be rewritten as

$$\begin{cases} \begin{bmatrix} \delta\boldsymbol{x}_k(t+1) \\ \hat{\boldsymbol{e}}_{k+1}(t) \end{bmatrix} = \tilde{A} \begin{bmatrix} \delta\boldsymbol{x}_k(t) \\ \hat{\boldsymbol{e}}_k(t) \end{bmatrix} + B_1\delta\bar{\boldsymbol{u}}_k(t-1) \\ +B_2\delta\boldsymbol{f}_k(t), \\ \boldsymbol{z}_k(t) = C \begin{bmatrix} \delta\boldsymbol{x}_k(t) \\ \hat{\boldsymbol{e}}_k(t) \end{bmatrix}, t \in [1, T_f], k \geq 0, \end{cases} \tag{27}$$

where the system matrix is $\tilde{A} = A + B_1L$. Next, we will give the design criteria for learning gain matrix L.

Definition 2: The 2-D Roesser model (27) with boundary conditions (24) is said to have a 2-D guaranteed cost performance if it satisfies the following conditions:

$$\lim_{k\to\infty} \begin{bmatrix} \delta\boldsymbol{x}_k(t) \\ \hat{\boldsymbol{e}}_k(t) \end{bmatrix} = 0 \tag{28}$$

for $\forall t \in [1, T_f]$ when $\delta\bar{\boldsymbol{u}}_k(t) = 0$, and

$$\|\boldsymbol{z}_k(t)\|_2^2 \leq \gamma_1\|\delta\boldsymbol{x}_k(1)\|_2^2 + \gamma_2\|\hat{\boldsymbol{e}}_0(t)\|_2^2 + \gamma_3\|\delta\bar{\boldsymbol{u}}_k(t)\|_2^2 \tag{29}$$

for any norm bounded $\delta\bar{\boldsymbol{u}}_k(t)$, where $\gamma_1, \gamma_2, \gamma_3 > 0$.

Theorem 1: Given a positive scalar γ, the 2-D system (27) with restrictions (24) has a guaranteed cost performance γ if and only if there exist a symmetric positive definite matrix $X \triangleq X_h \bigoplus X_v, X_h \in \mathbb{R}^{2\times2}, X_v \in \mathbb{R}^{\varrho\times\varrho}$ and a matrix $Y \in \mathbb{R}^{2\times(\varrho+2)}$ satisfying the following linear matrix inequality (LMI):

$$\begin{bmatrix} -X & \prod_0 & B_1 + l_2B_2 & 0 \\ * & -X & 0 & XC^T \\ * & * & -\gamma^2 I_2 & 0 \\ * & * & * & -I_\varrho \end{bmatrix} < 0, \tag{30}$$

where $\prod_0 = AX + B_1Y + B_2L_1X, L_1 = [l_1I_2, 0]$ and the learning gain matrix is $L = YX^{-1}$.

Proof. See Appendix A.

Remark 2: The HOIM-based MPILC law (21) and (26) has fully utilized the historical driving information, tracking error and the future state information during the prediction horizon. Therefore, the MPILC law for PHEV can provide a better performance than MPC or ILC.

Then, the control task is changed to find an optimal compensation $\delta\bar{\boldsymbol{u}}_k(t)$ in the MPILC (26) such that the FC and battery aging are balanced.

D. NONLINEAR OPTIMIZATION

The nonlinear optimization for the torque split problem can be defined as a weighted sum of FC, battery aging and deviation of SOC within k iteration:

$$\begin{aligned}\underset{\delta\bar{\boldsymbol{u}}_k(t)}{arg\,min}\ J_k &= (1-\lambda)\sum_{t=t_0}^{p+t_0}\dot{m}_f(\boldsymbol{u}_k(t), T_{d,k}(t)) \\ &+\lambda\sum_{t=t_0}^{p+t_0}\frac{c_a}{\Gamma}\{\left|I_c(\boldsymbol{u}_k(t), T_{d,k}(t))\right| \cdot \\ &\sigma_{map}[I_c(\boldsymbol{u}_k(t), T_{d,k}(t)), \theta_k(t)]\} \\ &+\lambda_0\sum_{t=t_0}^{p+t_0}|SOC_k(t) - SOC_r(t)|, \end{aligned} \tag{31}$$

where J_k is the cost function. $\lambda \in [0, 1]$ is a parameter to balance the two objectives: minimization of FC and battery fading. c_a is a transformation coefficient that makes the amount of battery aging dimensionally compatible with FC, and it can be defined as a ratio of battery replacement cost to that of 1kg of fuel [24]. λ_0 is equivalent coefficient of deviation of SOC. $p = 10$ is predictive horizon. t_0 is the current time, i.e., the starting point of prediction horizon. It is worth mentioning that the objective (31) with constraints (19) is very complex and its analytical expressions is even unacquirable. To reduce computational burden, it is solved by an improved dynamic programming (IDP) method [8], [17], [46]. The core idea includes two main aspects. First, we take full advantage of the relationship between SOC and power of electric machine (6) and the dimension reduction technique is adopted. Then, SOC is the unique free variable in IDP. Second, the feasible region of SOC is small, and its boundary of each step can be calculated with the maximum and minimum power of electric machine. Therefore, the region of the state variable of IDP is decreased which means a reduced computational burden.

Remark 3: It can be seen that there are three terms in the cost function (31), of which the first is FC, the second is equivalent battery cost and the third is a limit to the SOC operating region. Therefore, the EMS based on nonlinear optimization can improve the fuel economy and battery life span simultaneously.

E. PROPERTY ANALYSIS

According to the theorem 1, the 2-D system (27) has a guaranteed cost performance γ for any norm bounded $\delta\bar{\boldsymbol{u}}_k(t)$. Design a reasonable objective as

$$\mathbb{J}(\zeta) = \sum_{k=0}^{\infty}\sum_{t=0}^{T_f} J_k(t)$$

where $\zeta \in \{MPILC, ILC, MPC\}$ represents the controller type.

Firstly, due to $\delta\bar{\boldsymbol{u}}_k(t)$ is the optimal solution of the minimization problem (31), and the MPILC (26) is reduced to an ILC when $\delta\bar{\boldsymbol{u}}_k(t) = 0$, then, we have

$$\mathbb{J}(MPILC) \le \mathbb{J}(ILC), \tag{32}$$

which implies that the smaller FC, more moderate battery aging and more perfect asymptotically tracking can be achieved easier by utilizing MPILC law than that by utilizing ILC. Without the iterative learning, the same tracking errors and defects will emerge repeatedly and not converge along with the iterative axis as the same working condition of PHEV are repeated, hence,

$$\mathbb{J}(MPILC) \le \mathbb{J}(MPC), \tag{33}$$

which implies that the performance of PHEV by utilizing MPILC is better than that by utilizing MPC.

Remark 4: According to (32) and (33), combined the advantages of MPC and ILC, the MPILC law (26) is very useful to improve tracking performance, accelerate convergence speed, overcome model error and measurement noise.

F. MPILC FOR PHEV

For the PHEV running in city route, driver behaviors in the near future are stochastic but iterative repetitiveness and periodicity. To fully use the historical information during the past week, an MPILC is proposed, which could get the optimal control sequence over a finite time region during every operational cycle of PHEV, and make a batch-to-batch improvements during different cycles [47]. And the HOIM-based MPILC is given as

$$\begin{cases}\boldsymbol{u}_{k+1}(t) = G_{\varrho}(q^{-1})\boldsymbol{u}_k(t) + \delta\bar{\boldsymbol{u}}_{k+1}(t) \\ +L[\delta\boldsymbol{x}_k^T(t+1)\hat{\boldsymbol{e}}_k^T(t+1)]^T, k \ge 0, \\ \boldsymbol{u}_k(t) = \boldsymbol{u}_0(t), k \le 0.\end{cases} \tag{34}$$

Remark 5: The historical working condition information has been fully used to improve the performance of PHEV, not only the HOIM-based driver model (12), but also the iterative learning compensation of the historical tracking error. Therefore, the proposed MPILC (34) can provide a more reasonable control input to achieve a perfect performance for PHEV.

IV. SIMULATION AND RESULTS ANALYSIS

In this section, the MPILC, which considers the historical driver information and battery aging, is adopted for the optimal energy management of PHEV. The framework is shown in Figure 5. It can be found that the framework can be divided into three main parts. The first part is the demand torque and reference SOC obtained from historical data. The second part is the nonlinear optimization to balance FC and battery aging. The last part is the proposed MPILC law for PHEV. According to the PHEV parameters, we have $l_1 = 2.84 \times 10^{-4}$, $l_2 = 1.26 \times 10^{-5}$. Selecting $\gamma = 0.5$, the learning gain matrix calculated by (30) is

$$L = -\begin{bmatrix} 49.1688 & 0.5235 & 0.2480 & 0.2122 \\ 49.1751 & 0.5235 & 0.2481 & 0.2122 \\ 0.1766 & 0.1411 & 0.1057 & 0.0705 & 0.0353 \\ 0.1766 & 0.1411 & 0.1058 & 0.0705 & 0.0353 \end{bmatrix}.$$

To verify the performance of the proposed MPILC, a real driving cycle collected from a city bus line in Xiamen city

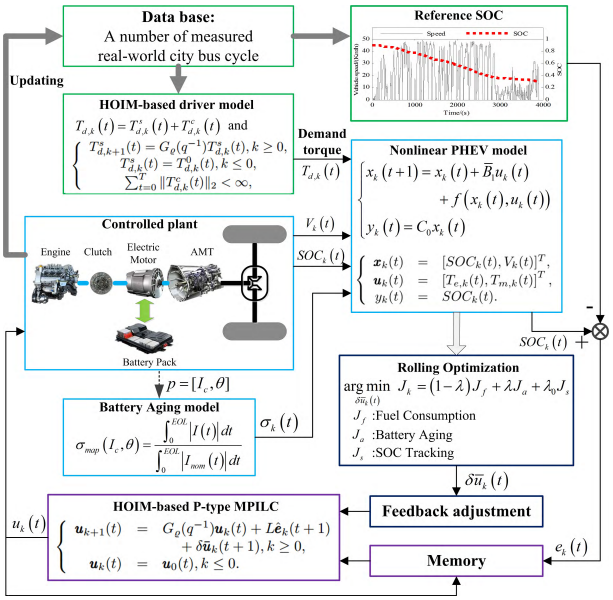

FIGURE 5. Framework of the MPILC.

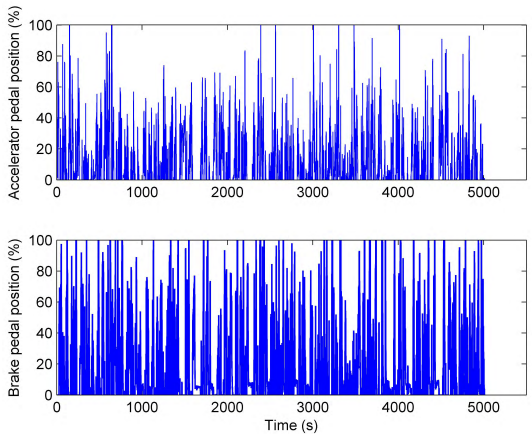

FIGURE 6. Pedal positions of a real driving cycle.

is adopted, where the original pedal positions are measured from a real bus with travel length 23.324km and travel time 5010s as shown in Figure 6. We add some driver and transportation disturbances into the driving cycle and the disturbances are different every day, we also repeat it 30 times, which imitates the real repeating transportation scenarios during one month. In particular, there are more than one traffic jam, twice emergent obstacles and triple red lights disturbances during every day, respectively. For the driving cycle of the 30^{th} iteration as an example, the representational transportation disturbances are traffic jam during 2400s-3000s, emergent obstacles during 1620s-1680s and 4080s-4140s, and red lights during 980s-1010s, 2240s-2300s and 4420s-4480s.

For simplicity, we only give some results as representatives. The results including vehicle speeds, engine torques, motor torques and SOCs of the 30^{th} iteration are shown in Figure 7, respectively. It can be seen that the hybrid powertrain system can meet the torque demand of driver by the optimal splits obtained by the MPILC. Moreover, the battery

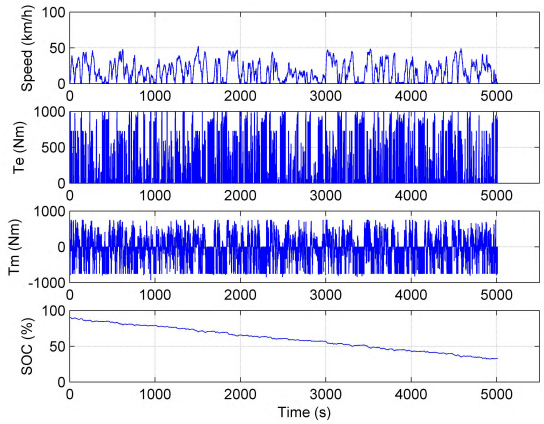

FIGURE 7. Results of the 30^{th} iteration.

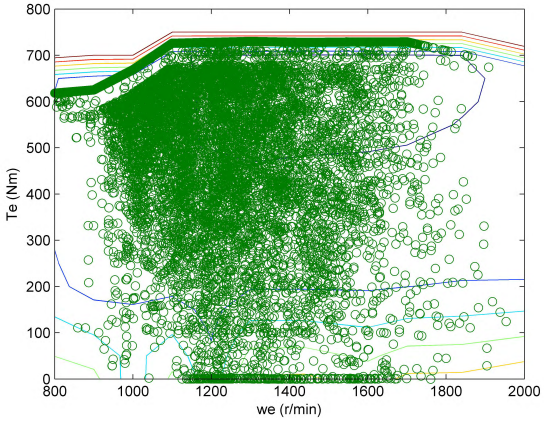

FIGURE 8. Engine operating points of the first iteration.

energy is just exhausted during the entire bus line in order to make full use of the energy from power grid.

As we known, the FC of PHEV is mainly determined by the engine operating condition. From the results of the real bus driving cycle, the engine operating conditions are shown in Figures 8-11. It is obvious that there are more operating points in low efficient zone in the beginning stages than that in the later stages. And the numbers of operating points in high efficient zone will be increased along with the iteration processing, which is the essential reason why the FC will be better after some trials with the key idea of 'practice makes perfect'. And it is manifested again in the iteration results of FC and SOC average error shown in Figure 12. Through the desirable torque split between engine and motor, the proper operating modes and optimal fuel economy could be achieved along the driving cycles. Then, the engine is guaranteed to be working in high efficient zone. Therefore, combined the iterative learning and optimization techniques, the MPILC-based EMS will provide a better fuel economy with a satisfying computation burden.

According to Figure 12, the FC will be reduced from 17.08L/100km to 14.89L/100km after 19 iterations with 12.82% improvement. To further express the effectiveness of the proposed method, we perform the rule-based [6] and DP-based [8] methods again with the same driving cycle

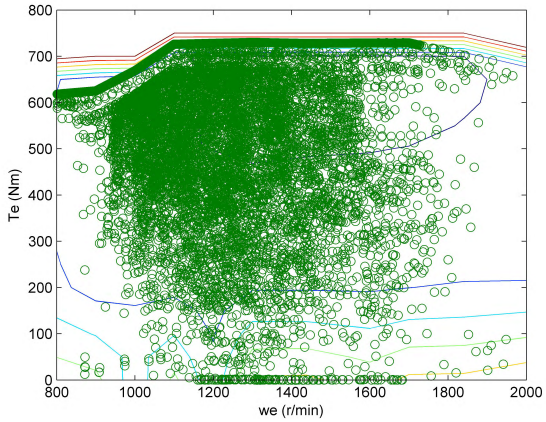

FIGURE 9. Engine operating points of the 10^{th} iteration.

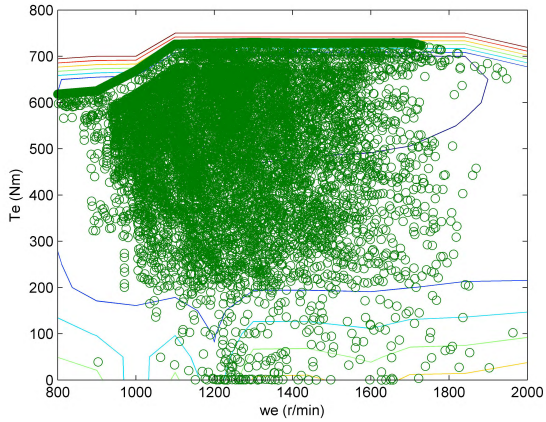

FIGURE 10. Engine operating points of the 20^{th} iteration.

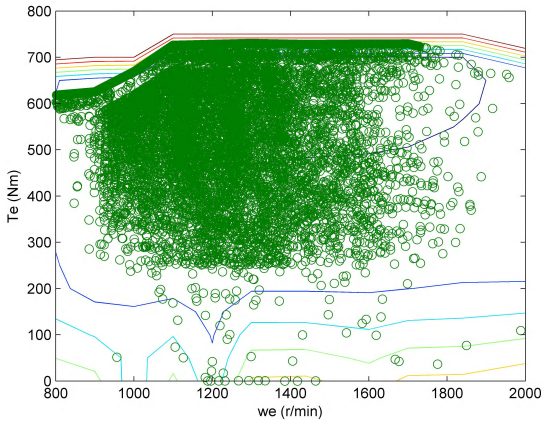

FIGURE 11. Engine operating points of the 30^{th} iteration.

which are without learning from the historical driving information, and the corresponding minimal FCs without learning are 20.51L/100km and 14.29L/100km, respectively. The FC obtained by MPILC has a 27.4% improvement compared to the FC obtained by rule-based method without learning and a 4.2% deterioration compared to the DP-based method without learning, respectively. And the improvement effects on battery fading are more obvious, especially after 30 driving cycles, the battery fading obtained by MPILC has a 37.1%

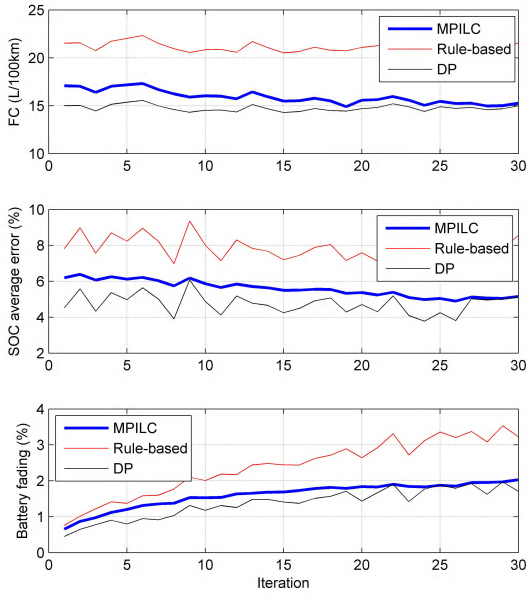

FIGURE 12. Iteration results.

improvement compared to rule-based method without learning. The performances obtained by DP-based method without learning are the best one of these three methods, nevertheless, the huge computation burden of DP is a significant drawback for real-time application [9]. It is easy to recognize that the performance of MPILC is better and better and it approaches to that of DP after some iterations. Hence, the proposed MPILC is verified with better performances in both FC, battery health, robustness and real-time processing capacity.

To further validate the effectiveness and robustness of the proposed method, we perform it again and apply on another different routes during the 10^{th} and 15^{th} iterations, and also some more disturbances are added in the driving cycles. The transportation disturbances are listed in Table 2 and the learning process is shown as Figure 13. According to the results, the FC is reduced from 17.08L/100km to 15.79L/100km after 28 iterations with 7.56% improvement. It is obvious that the performance with other different routes or drivers will be worse provisionally. However, the advantages of the

TABLE 2. Traffic lights of the scenes.

Iterations	1th	2th	3th	4th	5th	6th
Numbers of red lights	27	27	25	28	27	27
Iterations	7th	8th	9th	10th	11th	12th
Numbers of red lights	27	27	25	24	27	26
Iterations	13th	14th	15th	16th	17th	18th
Numbers of red lights	27	24	26	28	28	27
Iterations	19th	20th	21th	22th	23th	24th
Numbers of red lights	26	25	25	26	27	24
Iterations	25th	26th	27th	28th	29th	30th
Numbers of red lights	28	27	25	27	27	25

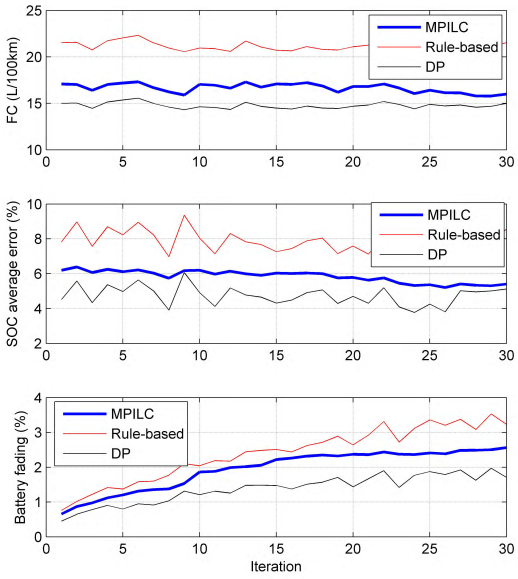

FIGURE 13. Iteration results with different routes.

proposed MPILC have been reflected. The most important characteristic is that it can handle well the varying transportation scenes by iterative learning and model-based predicting. As we can see that, after a red light disturbance or emergent obstacle, the vehicle will stop or brake, and some energy will be wasted. Nevertheless, the robustness performance has been validated by the iterative convergence process. We can infer that the performances of MPILC will approach to that of DP after some more iterations. During these learning process, FCs and SOC errors will express an imperceptible and gradual downtrend although there are some disturbances especially for a different route or driver. According to the results discussed above, the proposed MPILC is practical due to the consideration of the variation of cycle duration in the HOIM-based driver model (12) and (13). Furthermore, the effectiveness and robustness are verified more reasonably.

V. CONCLUSION

Based on the 2-D Lyapunov stability theory, a uniform scheme for the combination of ILC and MPC is presented in this paper. A novel MPILC is proposed based on the iterative learning and model predicting from the historical driving data. By involving the within-batch MPC into a batch-to-batch ILC by minimizing a nonlinear cost function, the PHEV can illustrate a perfect performance in FC, battery health, robustness and real-time processing capacity. The proposed MPILC for the optimal torque split in PHEV is demonstrated by a real driving cycle collected from a bus line in Xiamen city. Above all, a new attempt for EMS is established to minimize FC and battery degradation.

APPENDIX A
PROOF OF THE THEOREM 3.1

Let $R_h = X_h^{-1}, R_v = X_v^{-1}, R \triangleq R_h \bigoplus R_v$, then, according to Schur Complement theorem, the inequality (30) is equivalent to

$$\Psi = \begin{bmatrix} \prod + C^T C & \Psi_{12} \\ * & \Psi_{22} \end{bmatrix} < 0, \tag{35}$$

where $\prod = \tilde{A}^T R\tilde{A} + \tilde{A}^T RB_2L_1 + L_1^T B_2^T R\tilde{A} + L_1^T B_2^T RB_2L_1 - R$, $\Psi_{12} = \tilde{A}^T RB_1 + l_2\tilde{A}^T RB_2 + L_1^T B_2^T RB_1 + l_2L_1^T B_2^T RB_2$, $\Psi_{22} = B_1^T RB_1 + l_2B_2^T RB_1 + l_2B_1^T RB_2 + l_2^2B_2^T RB_2 - \gamma^2 I_2$. Firstly, a Lyapunov analysis method is employed to prove the asymptotic stability of the 2-D system (27) with $\delta\bar{\boldsymbol{u}}_k(t) = 0$. For convenience, let $\boldsymbol{x}_1 = [\delta\boldsymbol{x}_k^T(t), \hat{\boldsymbol{e}}_k^T(t)]^T, \boldsymbol{x}_2 = [\delta\boldsymbol{x}_k^T(t+1), \hat{\boldsymbol{e}}_{k+1}^T(t)]^T = \tilde{A}\boldsymbol{x}_1 + B_1\delta\bar{\boldsymbol{u}}_k(t) + B_2\delta\boldsymbol{f}_k(t)$, and $V(\boldsymbol{x}) = \boldsymbol{x}^T R\boldsymbol{x}$. Then, the difference $\Delta V_x = V(\boldsymbol{x}_2) - V(\boldsymbol{x}_1)$ with $\delta\bar{\boldsymbol{u}}_k(t) = 0$ yields

$$\Delta V_x \le \boldsymbol{x}_1^T \prod \boldsymbol{x}_1, \tag{36}$$

where $\prod < 0$ is implied in the inequality (35). It follows that $\Delta V_x \le 0$. Note that

$$\begin{aligned}\Delta V_x = {} & \delta\boldsymbol{x}_k^T(t+1)R_h\delta\boldsymbol{x}_k(t+1) - \delta\boldsymbol{x}_k^T(t)R_h\delta\boldsymbol{x}_k(t) \\ & + \hat{\boldsymbol{e}}_{k+1}^T(t)R_v\hat{\boldsymbol{e}}_{k+1}(t) - \hat{\boldsymbol{e}}_k^T(t)R_v\hat{\boldsymbol{e}}_k(t),\end{aligned} \tag{37}$$

then, we have $\sum_{k=0}^{p}\sum_{t=1}^{q}\Delta V_x = \sum_{k=0}^{p}[\delta\boldsymbol{x}_k^T(q+1)R_h\delta\boldsymbol{x}_k(q+1) - \delta\boldsymbol{x}_k^T(1)R_h\delta\boldsymbol{x}_k(1)] + \sum_{t=1}^{q}[\hat{\boldsymbol{e}}_{p+1}^T(t)R_v\hat{\boldsymbol{e}}_{p+1}(t) - \hat{\boldsymbol{e}}_0^T(t)R_v\hat{\boldsymbol{e}}_0(t)] \le 0$ for $\forall p \ge 0, q \in [1, T_f]$, which follows that

$$\begin{aligned}\sum_{k=0}^{p}\delta\boldsymbol{x}_k^T(q+1)R_h\delta\boldsymbol{x}_k(q+1) & \\ < \sum_{k=0}^{p}\delta\boldsymbol{x}_k^T(1)R_h\delta\boldsymbol{x}_k(1) & + \sum_{t=1}^{q}\hat{\boldsymbol{e}}_0^T(t)R_v\hat{\boldsymbol{e}}_0(t).\end{aligned}$$

According to the boundary condition (24), we can see $\sum_{k=0}^{\infty}\delta\boldsymbol{x}_k^T(q+1)R_h\delta\boldsymbol{x}_k(q+1) < \infty$ for $\forall q \in [1, T_f]$. It implies that $\lim_{k\to\infty}\delta\boldsymbol{x}_k(t) = 0$ for $\forall t \in [1, T_f]$.

Next, we will prove $\lim_{k\to\infty}\hat{\boldsymbol{e}}_k(t) = 0$ for $\forall t \in [1, T_f]$. Note that $\hat{\boldsymbol{e}}_k^T(t)R_v\hat{\boldsymbol{e}}_k(t) \le \lambda_{\max}(R_v)\|\hat{\boldsymbol{e}}_k(t)\|_2^2 < [\lambda_{\max}(R_v) + \lambda_{\min}(-\prod)]\|\hat{\boldsymbol{e}}_k(t)\|_2^2$ and $\Delta V_x \le -\lambda_{\min}(-\prod)\cdot\|\hat{\boldsymbol{e}}_k(t)\|_2^2$, then, we can obtain

$$\Delta V_x < -\gamma_0\hat{\boldsymbol{e}}_k^T(t)R_v\hat{\boldsymbol{e}}_k(t), \tag{38}$$

where $\gamma_0 = \frac{\lambda_{\min}(-\prod)}{\lambda_{\max}(R_v)+\lambda_{\min}(-\prod)} \in (0, 1)$. From (37) and (38), we have $\hat{\boldsymbol{e}}_{k+1}^T(t)R_v\hat{\boldsymbol{e}}_{k+1}(t) < \delta\boldsymbol{x}_k^T(t)R_h\delta\boldsymbol{x}_k(t) - \delta\boldsymbol{x}_k^T(t+1)R_h\delta\boldsymbol{x}_k(t+1) + (1-\gamma_0)\hat{\boldsymbol{e}}_k^T(t)R_v\hat{\boldsymbol{e}}_k(t)$, which implies that $\sum_{t=1}^{T_f}\hat{\boldsymbol{e}}_{k+1}^T(t)R_v\hat{\boldsymbol{e}}_{k+1}(t) < \delta\boldsymbol{x}_k^T(1)R_h\delta\boldsymbol{x}_k(1) + (1-\gamma_0)\sum_{t=1}^{T_f}\hat{\boldsymbol{e}}_k^T(t)R_v\hat{\boldsymbol{e}}_k(t)$ for $\forall k \ge 0$. It follows that $\sum_{t=1}^{T_f}\hat{\boldsymbol{e}}_k^T(t)R_v\hat{\boldsymbol{e}}_k(t) < (1-\gamma_0)^k\sum_{t=1}^{T_f}\hat{\boldsymbol{e}}_0^T(t)R_v\hat{\boldsymbol{e}}_0(t) + \sum_{j=0}^{k-1}[(1-\gamma_0)^{k-1-j}\delta\boldsymbol{x}_j^T(1)R_h\delta\boldsymbol{x}_j(1)]$ for $\forall k \ge 1$. Then,

$$\begin{aligned}\sum_{k=0}^{\infty}\sum_{t=1}^{T_f}\hat{\boldsymbol{e}}_k^T(t)R_v\hat{\boldsymbol{e}}_k(t) < {} & \frac{1}{\gamma_0}\sum_{t=1}^{T_f}\hat{\boldsymbol{e}}_0^T(t)R_v\hat{\boldsymbol{e}}_0(t) \\ & + \frac{1}{\gamma_0}\sum_{k=0}^{\infty}\delta\boldsymbol{x}_k^T(1)R_h\delta\boldsymbol{x}_k(1),\end{aligned}$$

which implies $\sum_{k=0}^{\infty}\sum_{t=1}^{T_f}\hat{\boldsymbol{e}}_k^T(t)R_v\hat{\boldsymbol{e}}_k(t)<\infty$. It follows that $\lim_{k\to\infty}\hat{\boldsymbol{e}}_k(t)=0$ for $\forall t\in[1,T_f]$.

Therefore, the asymptotic stability of the 2-D system (27) with $\delta\bar{\boldsymbol{u}}_k(t)=0$ is proved. Next, we will further exhibit the 2-D guaranteed cost performance when MPILC (26) is applied. Construct a function $J(k,t)=\Delta V_x+\hat{\boldsymbol{e}}_k^T(t)\hat{\boldsymbol{e}}_k(t)-\gamma^2\delta\bar{\boldsymbol{u}}_k^T(t-1)\delta\bar{\boldsymbol{u}}_k(t-1)$. According to (25) and (26), we have

$$J(k,t)\le\boldsymbol{\xi}^T(k,t)\Psi\boldsymbol{\xi}(k,t)\le 0, \tag{39}$$

where $\boldsymbol{\xi}(k,t)=[\boldsymbol{x}_1^T,\delta\bar{\boldsymbol{u}}_k^T(t-1)]^T$ and $\Psi<0$ is equivalent to the inequality (30). Moreover, we can get $\sum_{k=0}^{\infty}\sum_{t=1}^{T_f}J(k,t)\le-\lambda_{\min}(-\Psi)\|\delta\bar{\boldsymbol{u}}_k(t)\|_2^2$, and $\sum_{k=0}^{\infty}\sum_{t=1}^{T_f}\Delta V_x\ge-\lambda_{\max}(R_h)\|\delta\boldsymbol{x}_k(1)\|_2^2-\lambda_{\max}(R_v)\|\hat{\boldsymbol{e}}_0(t)\|_2^2$. Hence, it follows

$$\begin{aligned}\|\hat{\boldsymbol{e}}_k(t)\|_2^2\le{}&\lambda_{\max}(R_h)\|\delta\boldsymbol{x}_k(1)\|_2^2+\lambda_{\max}(R_v)\|\hat{\boldsymbol{e}}_0(t)\|_2^2\\&+[\gamma^2-\lambda_{\min}(-\Psi)]\|\delta\bar{\boldsymbol{u}}_k(t)\|_2^2,\end{aligned}$$

where $\delta\bar{\boldsymbol{u}}_k(t)$ is the within-batch part which is the globally optimal solution of the cost function (31). Then, $\delta\bar{\boldsymbol{u}}_k(t)$ is norm bounded. Therefore, the asymptotic stability along with time and iteration axes is guaranteed by the inequality (30) and the boundary condition (24). According to Definition 2, the proof is completed. □

REFERENCES

[1] C. M. Martinez, X. Hu, D. Cao, E. Velenis, B. Gao, and M. Wellers, "Energy management in plug-in hybrid electric vehicles: Recent progress and a connected vehicles perspective," *IEEE Trans. Veh. Technol.*, vol. 66, no. 6, pp. 4534–4549, Jun. 2017.

[2] L. Li, X. Wang, R. Xiong, K. He, and X. Li, "AMT downshifting strategy design of HEV during regenerative braking process for energy conservation," *Appl. Energy*, vol. 183, no. 1, pp. 914–925, Dec. 2016.

[3] Y. Du, Y. Zhao, Q. Wang, Y. Zhang, and H. Xia, "Trip-oriented stochastic optimal energy management strategy for plug-in hybrid electric bus," *Energy*, vol. 115, pp. 1259–1271, Nov. 2016.

[4] S. Uebel, N. Murgovski, C. Tempelhahn, and B. Bäker, "Optimal energy management and velocity control of hybrid electric vehicles," *IEEE Trans. Veh. Technol.*, vol. 67, no. 1, pp. 327–337, Jan. 2018.

[5] C. Zhang and A. Vahidi, "Route preview in energy management of plug-in hybrid vehicles," *IEEE Trans. Control Syst. Technol.*, vol. 20, no. 2, pp. 546–553, Mar. 2012.

[6] J. Peng, H. He, and R. Xiong, "Rule based energy management strategy for a series–parallel plug-in hybrid electric bus optimized by dynamic programming," *Appl. Energy*, vol. 185, pp. 1633–1643, Jan. 2017.

[7] N. Denis, M. R. Dubois, and A. Desrochers, "Fuzzy-based blended control for the energy management of a parallel plug-in hybrid electric vehicle," *IET Intell. Transp. Syst.*, vol. 9, no. 1, pp. 30–37, Feb. 2015.

[8] L. Li, C. Yang, Y. Zhang, L. Zhang, and J. Song, "Correctional DP-based energy management strategy of plug-in hybrid electric bus for city-bus route," *IEEE Trans. Veh. Technol.*, vol. 64, no. 7, pp. 2792–2803, Jul. 2015.

[9] X. Hu, N. Murgovski, L. Johannesson, and B. Egardt, "Energy efficiency analysis of a series plug-in hybrid electric bus with different energy management strategies and battery sizes," *Appl. Energy*, vol. 111, pp. 1001–1009, Nov. 2013.

[10] W. Wang, Z. Zhang, J. Shi, C. Lin, and Y. Gao, "Optimization of a dual-motor coupled powertrain energy management strategy for a battery electric bus based on dynamic programming method," *IEEE Access*, vol. 6, pp. 32899–32909, 2018.

[11] S. Zhang, R. Xiong, and F. Sun, "Model predictive control for power management in a plug-in hybrid electric vehicle with a hybrid energy storage system," *Appl. Energy*, vol. 185, pp. 1654–1662, Jan. 2017.

[12] Z. Chen, N. Guo, J. Shen, R. Xiao, and D. Peng, "A hierarchical energy management strategy for power-split plug-in hybrid electric vehicles considering velocity prediction," *IEEE Access*, vol. 6, pp. 33261–33274, 2018.

[13] Y. Huang, H. Wang, A. Khajepour, H. He, and J. Ji, "Model predictive control power management strategies for hevs: A review," *J. Power Sources*, vol. 341, pp. 91–106, Feb. 2017.

[14] A. Taghavipour, N. L. Azad, and J. McPhee, "Real-time predictive control strategy for a plug-in hybrid electric powertrain," *Mechatronics*, vol. 29, pp. 13–27, Aug. 2015.

[15] S. Di Cairano, D. Bernardini, A. Bemporad, and I. V. Kolmanovsky, "Stochastic MPC with learning for driver-predictive vehicle control and its application to HEV energy management," *IEEE Trans. Control Syst. Technol.*, vol. 22, no. 3, pp. 1018–1031, May 2014.

[16] Y. Zhang, L. Chu, Z. Fu, N. Xu, C. Guo, X. Zhang, Z. Chen, and P. Wang, "Optimal energy management strategy for parallel plug-in hybrid electric vehicle based on driving behavior analysis and real time traffic information prediction," *Mechatronics*, vol. 46, pp. 177–192, Oct. 2017.

[17] L. Li, S. You, C. Yang, B. Yan, J. Song, and Z. Chen, "Driving-behavior-aware stochastic model predictive control for plug-in hybrid electric buses," *Appl. Energy*, vol. 162, pp. 868–879, Jan. 2016.

[18] C. Sun, X. Hu, S. J. Moura, and F. Sun, "Velocity predictors for predictive energy management in hybrid electric vehicles," *IEEE Trans. Control Syst. Technol.*, vol. 23, no. 3, pp. 1197–1204, May 2015.

[19] L. Li, B. Yan, C. Yang, Y. Zhang, Z. Chen, and G. Jiang, "Application-oriented stochastic energy management for plug-in hybrid electric bus with AMT," *IEEE Trans. Veh. Technol.*, vol. 65, no. 6, pp. 4459–4470, Jun. 2016.

[20] P. Spagnol, S. Onori, N. Madella, Y. Guezennec, and J. Neal, "Aging and characterization of li-ion batteries in a hev application for lifetime estimation," *IFAC Proc. Volumes*, vol. 43, no. 7, pp. 186–191, Jul. 2010.

[21] T. Yuksel, S. Litster, V. Viswanathan, and J. J. Michalek, "Plug-in hybrid electric vehicle $LiFePO_4$ battery life implications of thermal management, driving conditions, and regional climate," *J. Power Sources*, vol. 338, pp. 49–64, Jan. 2017.

[22] S. J. Moura, J. L. Stein, and H. K. Fathy, "Battery-health conscious power management in plug-in hybrid electric vehicles via electrochemical modeling and stochastic control," *IEEE Trans. Control Syst. Technol.*, vol. 21, no. 3, pp. 679–694, May 2013.

[23] R. Xiong, J. Cao, and Q. Yu, "Reinforcement learning-based real-time power management for hybrid energy storage system in the plug-in hybrid electric vehicle," *Appl Energy*, vol. 211, pp. 538–548, Feb. 2018.

[24] L. Serrao, S. Onori, A. Sciarretta, Y. Guezennec, and G. Rizzoni, "Optimal energy management of hybrid electric vehicles including battery aging," in *Proc. Amer. Control Conf.*, San Francisco, CA, USA, Jun./Jul. 2011, pp. 2125–2130.

[25] X. Hu, C. M. Martinez, and Y. Yang, "Charging, power management, and battery degradation mitigation in plug-in hybrid electric vehicles: A unified cost-optimal approach," *Mech. Syst. Signal Process.*, vol. 87, pp. 4–16, Mar. 2017.

[26] J. H. Lee, S. Natarajan, and K. S. Lee, "A model-based predictive control approach to repetitive control of continuous processes with periodic operations," *J. Process Control*, vol. 11, no. 2, pp. 195–207, Apr. 2001.

[27] N. Zsiga, S. van Dooren, P. Elbert, and C. H. Onder, "A new method for analysis and design of iterative learning control algorithms in the time-domain," *Control Eng. Pract.*, vol. 57, pp. 39–49, Dec. 2016.

[28] N. Ajjanaromvat and M. Parnichkun, "Trajectory tracking using online learning LQR with adaptive learning control of a leg-exoskeleton for disorder gait rehabilitation," *Mechatronics*, vol. 51, pp. 85–96, May 2018.

[29] J. H. Lee and K. S. Lee, "Iterative learning control applied to batch processes: An overview," *Control Eng. Pract.*, vol. 15, no. 10, pp. 1306–1318, Oct. 2007.

[30] L. Huang, Q. Zhang, L. Sun, and Z. Sheng, "Robustness analysis of iterative learning control for a class of mobile robot systems with channel noise," *IEEE Access*, vol. 7, pp. 34711–34718, 2019.

[31] X. Liu and X. Kong, "Nonlinear fuzzy model predictive iterative learning control for drum-type boiler–turbine system," *J. Process Control*, vol. 23, no. 8, pp. 1023–1040, Sep. 2013.

[32] X. Jin, "Fault-tolerant iterative learning control for mobile robots non-repetitive trajectory tracking with output constraints," *Automatica*, vol. 94, no. 8, pp. 63–71, Aug. 2018.

[33] D. C. Chae, I. Chin, K. S. Lee, H. Rho, H. Rhee, and J. H. Lee, "Integrated quality and tracking control of a batch PMMA reactor using a QBMPC technique," *Comput. Chem. Eng.*, vol. 24, no. 2, pp. 953–958, Jul. 2000.

[34] Q. Fei, Y. Deng, H. Li, J. Liu, and M. Shao, "Speed ripple minimization of permanent magnet synchronous motor based on model predictive and iterative learning controls," *IEEE Access*, vol. 7, pp. 31791–31800, 2019.

[35] H. Guo, Q. Sun, C. Wang, Q. Wang, and S. Lu, "A systematic design and optimization method of transmission system and power management for a plug-in hybrid electric vehicle," *Energy*, vol. 148, pp. 1006–1017, Apr. 2018.
[36] C. Yang, J. Song, L. Li, S. Li, and D. Cao, "Economical launching and accelerating control strategy for a single-shaft parallel hybrid electric bus," *Mech. Syst. Signal Process.*, vols. 76–77, pp. 649–664, Aug. 2016.
[37] X. Zeng, N. Yang, J. Wang, D. Song, N. Zhang, M. Shang, and J. Liu, "Predictive-model-based dynamic coordination control strategy for power-split hybrid electric bus," *Mech. Syst. Signal Process.*, vols. 60–61, pp. 785–798, Aug. 2015.
[38] C. Liu, Q. Zhu, L. Li, W. Liu, L. Wang, N. Xiong, and X. Wang, "A state of charge estimation method based on H_∞ observer for switched systems of lithium-ion nickel–manganese–cobalt batteries," *IEEE Trans. Ind. Electron.*, vol. 64, no. 10, pp. 8128–8137, Oct. 2017.
[39] M. Berecibar, M. Garmendia, I. Gandiaga, J. Crego, and I. Villarreal, "State of health estimation algorithm of lifepo$_4$ battery packs based on differential voltage curves for battery management system application," *Energy*, vol. 103, pp. 784–796, May 2016.
[40] H. He, R. Xiong, H. Guo, and S. Li, "Comparison study on the battery models used for the energy management of batteries in electric vehicles," *Energy Convers. Manage.*, vol. 64, pp. 113–121, Dec. 2012.
[41] A. Sciarretta and L. Guzzella, "Control of hybrid electric vehicles," *IEEE Control Syst.*, vol. 27, no. 2, pp. 60–70, Apr. 2007.
[42] G. Suri and S. Onori, "A control-oriented cycle-life model for hybrid electric vehicle lithium-ion batteries," *Energy*, vol. 96, pp. 644–653, Feb. 2016.
[43] X. Zeng and J. Wang, "A two-level stochastic approach to optimize the energy management strategy for fixed-route hybrid electric vehicles," *Mechatronics*, vol. 38, pp. 93–102, Sep. 2016.
[44] Q. Zhu, J.-X. Xu, D. Huang, and G.-D. Hu, "Iterative learning control design for linear discrete-time systems with multiple high-order internal models," *Automatica*, vol. 62, pp. 65–76, Dec. 2015.
[45] C. Du and L. Xie, *H_∞ Control and Filtering of Two-Dimensional Systems* (Lecture notes in control and information sciences). Berlin, Germany: Springer-Verlag, 2002.
[46] L. Li, S. You, and C. Yang, "Multi-objective stochastic MPC-based system control architecture for plug-in hybrid electric buses," *IEEE Trans. Ind. Electron.*, vol. 63, no. 8, pp. 4752–4763, Aug. 2016.
[47] Z. Wang, C. P. Pannier, K. Barton, and D. J. Hoelzle, "Application of robust monotonically convergent spatial iterative learning control to microscale additive manufacturing," *Mechatronics*, vol. 56, pp. 157–165, Dec. 2018.

HONG-QIANG GUO received the Ph.D. degree in mechanical engineering from the Beijing Institute of Technology, China, in 2014. He is currently a Lecturer with the School of Mechanical and Automotive Engineering, Liaocheng University, Shandong, China. His research interests include hybrid powertrain system and control, and intelligent vehicle dynamics and control.

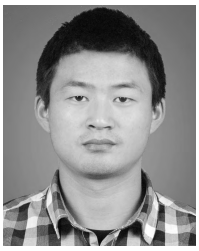

CONG-ZHI LIU received the B.S. degree in vehicle engineering from Southwest Jiaotong University, Chengdu, China, in 2013, and the M.S. degree in vehicle engineering from the Automotive Research Institute, Southwest Jiaotong University, in 2017. He is currently pursuing the Ph.D. degree in automotive engineering with the Department of Automotive Engineering, Tsinghua University, Beijing, China. His research interests include control theory and electric vehicle.

JIA-WANG YONG received the Ph.D. degree in automotive engineering from Beihang University, China, in 2017. He is currently a Postdoctoral Fellow with Tsinghua University in the field of automotive engineering. He has extensive experience in the design and development of electric brake systems, battery management systems, and vehicle-driver-road interaction analysis systems. His research interests include vehicle system dynamics and control, autonomous vehicle control, electric brake systems, and precision motion control.

XING-QUN CHENG received the Ph.D. degree in mechanical engineering from the Beijing Institute of Technology, China, in 2016. Then, he was engaged in postdoctoral research with the Beijing Institute of Technology, from 2016 to 2018. He is currently a Lecturer with the School of Mechanical and Automotive Engineering, Liaocheng University, Shandong, China. His research interests include dynamics control for electric vehicles and intelligent vehicles.

FAHAD MUHAMMAD received the Master of Mechanical Engineering in automotive engineering from Tsinghua University, Beijing, China, in 2016, where he is currently pursuing the Ph.D. degree in mechanical engineering with the Department of Automotive Engineering. His research interests include control theory and electric vehicles.